Mon. Not. R. Astron. Soc. **371,** 1113–1124 (2006) doi:10.1111/j.1365-2966.2006.10793.x

Optical and infrared diagnostics of SDSS galaxies in the SWIRE survey

P. Davoodi,[1⋆] F. Pozzi,[2] S. Oliver,[1] M. Polletta,[3] A. Afonso-Luis,[4] D. Farrah,[5] E. Hatziminaoglou,[4] G. Rodighiero,[6] S. Berta,[6] I. Waddington,[1] C. Lonsdale,[3,7] M. Rowan-Robinson,[8] D. L. Shupe,[9] T. Evans,[7] F. Fang,[9] H. E. Smith[3] and J. Surace[9]

[1]*Astronomy Centre, Department of Physics and Astronomy, University of Sussex, Brighton BN1 9QH*
[2]*Dipartimento di Astronomia, Università di Bologna, viale Berti Pichat 6, I-40127 Bologna, Italy*
[3]*Center for Astrophysics & Space Sciences, University of California, San Diego, La Jolla, CA 92093-0424, USA*
[4]*Instituto de Astrofísica de Canarias, Via Lactea S/N, E-38200, La Laguna, Spain*
[5]*Department of Astronomy, Cornell University, Ithaca, NY 14853, USA*
[6]*Dipartimento di Astronomia, Università di Padova, Vicolo dell'Osservatorio 2, I-35122, Padova, Italy*
[7]*Infrared Processing and Analysis Center, California Institute of Technology, Pasadena, CA 91125, USA*
[8]*Astrophysics Group, Blackett Laboratory, Imperial College London, Prince Consort Road, London SW7 2BW*
[9]*Spitzer Science Center, California Institute of Technology, Pasadena, CA 91125, USA*

Accepted 2006 July 6. Received 2006 June 29; in original form 2006 March 29

ABSTRACT

We present the rest-frame optical and infrared colours of a complete sample of 1114 $z < 0.3$ galaxies from the Spitzer Wide-Area Infrared Extragalactic (SWIRE) Legacy Survey and the Sloan Digital Sky Survey (SDSS). We discuss the optical and infrared colours of our sample and analyse in detail the contribution of dusty star-forming galaxies and active galactic nuclei (AGN) to optically selected red sequence galaxies.

We propose that the optical $(g - r)$ colour and infrared $\log(L_{24}/L_{3.6})$ colour of galaxies in our sample are determined primarily by a bulge-to-disc ratio. The $(g - r)$ colour is found to be sensitive to the bulge-to-disc ratio for disc-dominated galaxies, whereas the $\log(L_{24}/L_{3.6})$ colour is more sensitive for bulge-dominated systems.

We identify ∼18 per cent (195 sources) of our sample as having red optical colours and infrared excess. Typically, the infrared luminosities of these galaxies are found to be at the high end of star-forming galaxies with blue optical colours. Using emission-line diagnostic diagrams, 78 are found to have an AGN contribution and 117 are identified as star-forming systems. The red $(g - r)$ colour of the star-forming galaxies could be explained by extinction. However, their high optical luminosities cannot. We conclude that they have a significant bulge component.

The number densities of optically red star-forming galaxies are found to correspond to ∼13 per cent of the total number density of our sample. In addition, these systems contribute ∼13 per cent of the total optical luminosity density, and 28 per cent of the total infrared luminosity density of our SWIRE/SDSS sample. These objects may reduce the need for 'dry mergers'.

Key words: galaxies: elliptical and lenticular, cD – galaxies: evolution – galaxies: formation – infrared: galaxies.

1 INTRODUCTION

The global star formation history of the Universe can be investigated by combining ultraviolet and optical wavelength information with the infrared (IR), probing different stages (unobscured and obscured) of star formation processes.

The IR satellite *IRAS* (*Infrared Astronomy Satellite*; Neugebauer et al. 1984) has probed the local universe to determine how a third of the optical light from normal galaxies is absorbed by dust, and how this fraction can become higher when galaxies with the most active star formation activity (luminous infrared galaxies; Saunders & Mirabel 1996) are considered. The *ISO* (*Infrared Space Observatory*) satellites (Kessler et al. 1996) extended this analysis, showing the importance of dust in the high-redshift universe (Elbaz et al. 1999; Gruppioni et al. 2002; Rowan-Robinson

⋆E-mail: payam@sussex.ac.uk

et al. 2004; Metcalfe et al. 2005; Lonsdale, Farrah & Smith 2006).

Likewise, several studies (Wang & Silk 1994; Hogg et al. 2004; McIntosh et al. 2005) have shown that optical colours alone are not sufficient to discriminate the nature of some galaxy samples. In the K20 survey (Cimatti et al. 2004), spectral classifications show how two distinct populations with similar optical/near-IR colours contribute to a population of extremely red objects (EROs) at high redshift ($z \sim 2$): (i) old stellar systems with no signs of star formation and (ii) dusty star-forming galaxies. Moreover, studies of dusty galaxies locally and at high redshift (Poggianti & Wu 2000; Rigopoulou et al. 2000; Flores et al. 2004) have shown that more than 70 per cent of the energy emitted by young stars is reprocessed in the IR, leaving no trace in the optical spectrum of these systems. Given these results, complementing optical studies with IR information has become a crucial part of improving our understanding of optically selected galaxy samples.

One of the main aims of this paper is to explore the IR colour distribution and thus the star formation activity and dust content of low-redshift galaxies as a function of their rest-frame optical colours. Results from Strateva et al. (2001), Blanton et al. (2003), Bell et al. (2003) and Baldry et al. (2004) indicate that the colour distribution of galaxies in the optical can be represented by a *bimodal* function. In other words, formation processes give rise to two dominant populations with different average colours and dispersions. Galaxies with red optical colours, the 'red sequence', are generally considered to be early-type galaxies. Their colours are the result of old, high-metallicity stellar populations with little ongoing star formation. In comparison, galaxies with blue optical colours, the 'blue sequence', are considered to be late-type galaxies, probing current star formation. This optical colour distribution is found to be bimodal at $z \leqslant 0.1$ (Strateva et al. 2001; Baldry et al. 2004), $z \sim 1$ (Bell et al. 2004) and at least out to $z \sim 2$ (Giallongo et al. 2005), clearly reflecting the broad differences in star formation histories over large redshift ranges.

Since most of the activity [e.g. star formation and/or active galactic nuclei (AGN) emission] in galaxies is hidden by dust, the bolometric luminosity of active systems in the local universe (see e.g. Soifer & Neugebauer 1991) and at high redshifts (e.g. Sanders et al. 2004) is mostly emitted in the IR. Therefore, probing this emission will give a clearer insight into the star formation activity in galaxies forming the two optical sequences, and allows us to investigate whether the luminosity density of local galaxies is underestimated in the optical.

To understand the nature of galaxies in the two sequences at low redshift, we study the IR properties of galaxies from the Spitzer Wide-Area Infrared Extragalactic (SWIRE) survey [1] (Lonsdale et al. 2003), associating sources with their optical counterparts from the Sloan Digital Sky Survey (SDSS; York et al. 2000). SWIRE, the largest of the six cycle-1 Spitzer Legacy programmes, is a wide-area imaging survey, mapping the distribution of spheroids, discs, starbursts and AGN and their evolution from $z \sim 3$ to the current epoch. The survey covers $\sim$49 deg^2 (in six fields) in all seven Spitzer bands: 3.6, 4.5, 5.8 and 8 μm with the Infrared Array Camera (IRAC; Fazio et al. 2004) and 24, 70 and 160 μm with the Multiband Imaging Photometer for Spitzer (MIPS; Rieke et al. 2004), detecting $\sim$2.5 million galaxies down to $f_{3.6\,\mu\mathrm{m}} \approx 5$ μJy.

The large area of SWIRE provides statistically significant population samples over enough volume cells that we can resolve the star formation history as a function of epoch and environment. Combined with data from SDSS, the largest optical spectroscopic survey currently available, we can select a large sample of galaxies and efficiently probe their optical and IR emission.

The paper is outlined as follows. Section 2 describes the IR and optical data used to construct our sample. Sections 3 and 4 discuss the techniques used to derive rest-frame luminosities and spectral classifications using diagnostic diagrams based on optical spectra. In Sections 5 and 6, we investigate the optical and IR colours of our SWIRE/SDSS sample. In Section 7, we analyse the properties of galaxies with red optical colours and high mid-IR emission, to determine how they differ from star-forming galaxies with blue optical colours. The number density and optical/IR luminosity density of the different populations in our sample are determined in Section 8. Section 9 presents discussions and conclusions. For this work, we use a cosmological model with $\Omega_0 = 0.3, \Omega_\Lambda = 0.7$, and a Hubble constant of $H_0 = 72$ km s^{-1} Mpc^{-1}.

2 THE DATA

We use IRAC (3.6, 4.5, 5.8 and 8.0 μm) and MIPS (24, 70 and 160 μm) catalogues from the northern SWIRE fields of Lockman, ELAIS-N1 and ELAIS-N2, cross-correlated with SDSS *ugriz* photometry and spectroscopic catalogues to provide a complete $13 \leqslant r \leqslant 17.5$ sample of 1114 galaxies at $z < 0.3$. The total survey area of the three northern SWIRE fields is $\sim$24 deg^2, of which the overlap with SDSS is $\sim$18 deg^2.

Here, we discuss the technical aspects of the SWIRE and SDSS data sets.

2.1 Lockman, ELAIS-N1 and ELAIS-N2

The SWIRE Lockman field is centred at $10^{\mathrm{h}}\,45^{\mathrm{m}}\,00^{\mathrm{s}} + 58^{\mathrm{d}}\,00^{\mathrm{m}}\,00^{\mathrm{s}}$, with coverage of $\sim$10.6 deg^2. IRAC (3.6, 4.5, 5.8 and 8 μm)+MIPS (24 μm) observations were performed on 2004 April and May.

The SWIRE ELAIS-N1 field is centred at $16^{\mathrm{h}}\,11^{\mathrm{m}}\,00^{\mathrm{s}} + 55^{\mathrm{d}}\,00^{\mathrm{m}}\,00^{\mathrm{s}}$, with coverage of $\sim$9 deg^2. IRAC+24-μm observations were performed in 2004 January and February.

The SWIRE ELAIS-N2 field is centred at $16^{\mathrm{h}}\,36^{\mathrm{m}}\,48^{\mathrm{s}} + 41^{\mathrm{d}}\,01^{\mathrm{m}}\,45^{\mathrm{s}}$, with coverage of $\sim$4 deg^2. IRAC+24-μm observations were performed in 2004 July.

The average 5σ depths of Lockman, ELAIS-N1 and ELAIS-N2 are 5.0, 9.0, 43, 40 and 311 μJy at 3.6, 4.5, 5.8, 8 and 24 μm, respectively (Surace et al. 2005), consistent with the 90 per cent completeness levels for source extraction. Fluxes were extracted in 5.8-arcsec radius apertures for IRAC ($\sim$2×the FWHM beam) and 12 arcsec for MIPS, using SExtractor (Bertin & Arnouts 1996). The absolute flux calibrations are correct within $\sim$10 per cent for IRAC and MIPS 24-μm channel data, and were confirmed for IRAC and MIPS 24 μm by comparison to Two-Micron All-Sky Survey (2MASS). Further discussion on the data processing is given by Surace et al. (2005), Surace et al. (in preparation) and Shupe et al. (in preparation).

The Lockman field contains 681 587 SWIRE sources. The fields of ELAIS-N1 and ELAIS-N2 contain 411 015 and 309 507 SWIRE sources, respectively. Therefore, our total SWIRE sample consists of $\sim$1.4 million sources surveyed over a total of $\sim$24 deg^2.

The 5σ depths of MIPS 70- and 160-μm data are 14 and 105 mJy in all three SWIRE fields, consistent with 60 per cent completeness levels for source extraction (Afonso-Luis et al., in preparation). Point-source response function (PRF) fluxes in both bands were extracted using apex. Further details on flux calibrations and source extraction can be found in Frayer et al. (2006) and Afonso-Luis

[1] www.ipac.caltech.edu/SWIRE/

et al. (in preparation). The Lockman, ELAIS-N1 and ELAIS-N2 fields contain 2397, 1130 and 2485 sources with 70-μm detections. With regards to 160-μm detections, the fields of Lockman, ELAIS-N1 and ELAIS-N2 contain 1076, 439 and 1106 sources.

2.2 SDSS data

The SDSS sample of spectroscopically observed galaxies (Strauss et al. 2002) taken from the third Data Release (DR3; Abazajian et al. 2004) was used to provide optical *ugriz* magnitudes and spectroscopic redshifts for our sample. The SDSS data provide full coverage of the SWIRE fields of Lockman and ELAIS-N2 but covers only a third of the ELAIS-N1 field. Since our initial analysis was carried out using DR3, we have continued to use DR3 since DR4 does not provide any additional coverage of the SWIRE fields.

To remove sources with unreliable redshifts from our optical sample, we eliminated sources with the following SDSS spectroscopic pipeline flags; ZWARNING $\neq 0$ (problem with the redshift fitting) and zConf <0.85 (low confidence in the spectroscopic redshift). To eliminate stars, sources were only considered if they had a spectroscopic object class specClass = GALAXY or QSO and spectroscopic redshift >0.001 (see Blanton et al. 2004). Approximately 5 per cent of the SDSS sample did not meet these criteria, and were therefore classified as stars. These sources were removed from the SDSS sample.

2.3 SDSS morphological and spectral classifiers

The SDSS collaboration provides three galaxy classifiers: C_r (r-band concentration index; Shimasaku et al. 2001; Strateva et al. 2001), Sérsic index (Blanton et al. 2003; Hogg et al. 2004) and eClass (Connolly et al. 1995; Connolly & Szalay 1999; Yip et al. 2004).

The r-band concentration index C_r is a morphological classifier, defined as the ratio of the radii containing 90 and 50 per cent of the Petrosian r-band galaxy light. Shimasaku et al. (2001) and Strateva et al. (2001) find reasonable correlation between qualitative morphological classifications and C_r, with a $C_r \geqslant 2.6$ selection for early-type galaxies.

Sérsic index is another parameter measuring galaxy morphology, derived by fitting the functional form $I(r) = I_0 \exp(-r^{1/n})$ (where n is the Sérsic index itself), to each galaxy surface brightness profile. Hogg et al. (2004) find that galaxies with purely exponential profiles (Sérsic index $n \sim 1$) are considered late type (i.e. disc dominated) while galaxies with a de Vaucouleurs profiles (Sérsic index $n \sim 4$) are considered early type (i.e. bulge dominated).

The SDSS single parameter spectral classifier eClass is based on principal component analysis, using cross-correlation with eigentemplates constructed from SDSS galaxy spectra. This parameter ranges from approximately -0.35 to 0.5 for early to late galaxies (Stoughton et al. 2002). Based on the work by Yip et al. (2004) where eClass is modelled as a function of the distribution of galaxy populations, galaxies with an eClass < -0.02 are considered to be early type.

For the initial work discussed in Section 5, we define galaxies with $C_r \geqslant 2.6$ and eClass < -0.02 as early type, and those with $C_r < 2.6$ and eClass $\geqslant -0.02$ as late type. However, there are also sources that do not satisfy both conditions. The Sérsic index will be used as an additional classifier, and will be discussed in Section 6.

2.4 SWIRE/SDSS sample association

SWIRE IRAC+24-μm band-merged catalogues for Lockman, ELAIS-N1 and ELAIS-N2 were initially matched with the SDSS catalogues. Using the r-band SDSS and the 3.6-μm SWIRE coordinates, a SWIRE galaxy within 1.5 arcsec of the SDSS coordinate is chosen as the best match. This search radius is similar to that used to match SWIRE optical and IR data sets (see Surace et al. 2005). Since our sample consists of bright sources, we have verified that such criteria are adequate for matching sources. The MIPS 70- and 160-μm source catalogues were then individually matched to the 3.6-μm SWIRE coordinates of the SWIRE/SDSS catalogue. The MIPS 70-μm source catalogue was matched with a search radius of 10 arcsec. Sources were checked by visual inspection, to eliminate the 70-μm detection of any SWIRE sources with more than one 24-μm counterpart (three sources). SWIRE/SDSS sources were then matched with the MIPS 160-μm data, using a search radius of 20 arcsec. No sources were found to have a 160-μm detection and more than one 70-μm counterpart. The resulting SWIRE/SDSS spectroscopic catalogue consisted of 1988 sources.

To obtain a low-redshift SWIRE/SDSS sample, we choose galaxies with $0.001 \leqslant z \leqslant 0.3$. Following Bell et al. (2003), galactic foreground extinction-corrected $13 \leqslant r \leqslant 17.5$ (Schlegel et al. 1998) magnitude limits are applied, since these limits will give a reasonably complete optical sample, as discussed in more detail by e.g. Stoughton et al. (2002), Strauss et al. (2002) and Blanton et al. (2001).

This produces a final spectroscopic sample of 1114 SWIRE/SDSS galaxies.

2.5 Photometry

Since we are analysing the distribution of SWIRE/SDSS galaxies at low redshift, we require a total measure of optical and IR flux for extended sources.

For SDSS *ugriz*, we use extinction-corrected Petrosian magnitudes for measuring the total flux of a galaxy, and model magnitudes for measuring colours (see Baldry et al. 2004).

Bright sources which make up our spectroscopic sample have relatively high signal-to-noise ratio measurements of their Petrosian magnitudes, and so are expected to be accurate to better than 0.05 mag (Strauss et al. 2002; Bell et al. 2003; Blanton et al. 2003). These magnitudes recover all of the flux of an exponential galaxy profile and about 80 per cent of the flux for a de Vaucouleurs profile (Blanton et al. 2001).

For measuring the colours of these sources, we use model magnitudes. These magnitudes are calculated using the best-fitting parameters of the light profile (i.e. de Vaucouleurs/exponential) in the r band applied to all other bands. Therefore, the light is measured consistently through the same aperture in all bands, allowing an unbiased comparison of galaxy colours in our sample.

To obtain a measure of the IR flux of our sample, we use Kron magnitudes for SWIRE 3.6–24 μm bands, since they give the integrated flux through a larger aperture than that used for aperture magnitudes (see Bertin & Arnouts 1996). They are therefore a better measure of total flux, being within ∼8 per cent of the total flux of a galaxy (Kron 1980). As mentioned in Section 2.1, PRF fluxes were used for 70- and 160-μm data sets. The difference between PRF fluxes and aperture fluxes for our sample was found to be negligible.

3 *K*-CORRECTIONS AND LUMINOSITIES

To derive rest-frame absolute magnitudes for our sample, we use the SED (spectral energy distribution) template fitting photometric

redshift code LE PHARE[2] (Ilbert et al. 2005). Since sources in our sample have spectroscopic redshifts, we only use this code to determine rest-frame magnitudes and for fitting the SED of sources with galaxy templates.

LE PHARE can determine rest-frame magnitudes either by using a measure of apparent magnitude in the same observed band (hereafter *Op*0), or by automatically choosing the apparent magnitude in the observed band closest to the rest-frame band (hereafter *Op*1). For example, at $z \geqslant 0.12$ we expect rest-frame g band to be redshifted to observer-frame r band. Similarly, at $z \geqslant 0.08$ rest-frame r band will be redshifted to observer-frame i band. Since we are using a direct measurement of the emitted flux in these observed bands instead of the best-fitting SED, this technique limits the dependency on galaxy templates which can be the main source of error and systematics in absolute magnitude measurements.

We test the robustness of our rest-frame magnitude estimates using a simulated 8 deg^2 catalogue from GALICS (Hatton et al. 2003). We extract from the GALICS/MOMAF data base 5103 sources with *ugriz* observer-frame magnitudes, 'true' rest-frame magnitudes and redshifts. Applying similar r-band magnitude and redshift cuts as for our main spectroscopic sample, gives us a test sample of 678 sources.

Using the 42 synthetic templates of GISSEL 98 (Bruzual and Charlot 1993), we derive *ugriz* rest-frame magnitudes for our GALICS sample using *Op*0 and *Op*1. We find the dispersion when using *Op*0 to be in the range $\sigma = 0.027$–0.031 mag for g and r band. However, *Op*1 is found to be in better agreement with the 'true' rest-frame magnitudes of GALICS, with a dispersion of 0.025–0.028 mag for g and r band. We therefore adopt *Op*1 for determining rest-frame optical magnitudes for our spectroscopic sample.

We compute the rest-frame luminosities νL_ν of sources in our sample at 3.6 μm ($L_{3.6}$) and at 24 μm (L_{24}). The LE PHARE code has been used with a SWIRE library of galaxy and AGN templates[3] (covering a broad wavelength range from 0.1 to 1000 μm) to fit the optical (*ugriz*) and IR (3.6, 4.5, 5.8, 8.0 and 24 μm) SED of each galaxy, allowing us to determine rest-frame magnitudes at 3.6 and 24 μm. We also compute the optical ($L_{\rm OPT}$) and IR ($L_{\rm IR}$) bolometric luminosities of sources in our sample. Optical luminosities are determined by fitting SWIRE templates to the optical (*ugriz*)+ 3.6-μm SED of each object, and integrating between optical u and z bands (0.3–0.9 μm). IR luminosities are determined by fitting the IR 5.8–160 μm SED of each object with the full range of Dale & Helou (2002) model template spectra (64 galaxy templates), and integrating between 8 and 1000 μm.

4 SPECTRAL LINE ANALYSIS

We use the traditional log([O III]/Hβ) against log([N II]/Hα) flux ratio BPT diagram (see e.g. Baldwin, Phillips & Terlevich 1981; Veilleux & Osterbrock 1987; Kewley et al. 2001; Miller et al. 2004) to determine whether galaxies in our sample are star forming, AGN or systems with quiescent emission. Diagnostic diagrams involving [S II]/Hα or [O I]/Hα flux ratios are considered less effective at determining the level of AGN contamination in star-forming galaxies – see Brinchmann et al. (2004). We therefore do not use these ratios in our analysis.

The wavelength separation between the emission lines making up each ratio is small enough that each ratio is relatively insensitive to reddening or flux calibration errors. The fluxes of these emission lines are determined using the fitted heights and σ of the lines as measured by the SDSS data analysis pipeline.

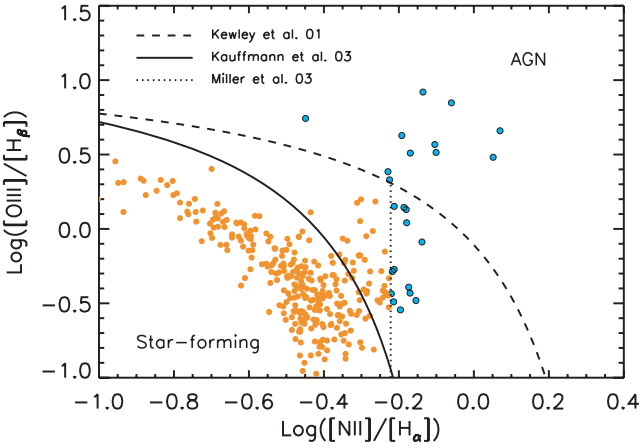

Figure 1. BPT (Baldwin et al. 1981) diagram in which the emission-line flux ratio [O III]/Hβ versus the ratio [N II]/Hα has been plotted for sources with emission-line detections above 3σ level. Cuts based on the models of Kewley et al. (2001) (dashed), Kauffmann et al. (2003) (solid) and Miller et al. (2004) (dotted) are illustrated. Galaxies are classified as star forming (orange) or AGN (cyan).

Initially, we consider sources with emission lines measurable at above 3σ level. Below this limit, a rapidly increasing fraction of galaxies will have a low significance detection in emission or absorption, leading to classification bias (Brinchmann et al. 2004). Fig. 1 shows a diagnostic diagram of 317 out of 1114 galaxies in our spectroscopic sample with emission-line detections above 3σ level in [O III], Hβ, Hα and [N II].

We adopt the emission-line classification criterion of Brinchmann et al. (2004), using a combination of three cuts to separate star-forming galaxies from AGN in this diagram. Galaxies below the solid line of Kauffmann et al. (2003) are expected to be star-forming systems with very low contribution to Hα from AGN. We find 257 galaxies lie below this line. The line of Kewley et al. (2001) (dashed) uses a combination of photoionization and stellar population synthesis models to place a conservative lower limit on the number of AGN in our sample. Galaxies with emission-line ratios that place them above the line of Kewley et al. (2001) cannot be explained by any possible combination of emission-line diagnostics that would be characteristic of a star-forming model (Kauffmann et al. 2003). 12 galaxies lie above this line, and we therefore classify these as AGN.

The remaining 48 out of 317 sources lie between the lines of Kauffmann et al. (2003) and Kewley et al. (2001). These are known as 'composite galaxies', since up to 40 per cent of their Hα luminosity may come from an AGN (Brinchmann et al. 2004). We therefore use the line of Miller et al. (2004) (dotted) in this region to try and classify the remaining composite galaxies as either star forming or AGN. For these galaxies to have an AGN contamination, they must have [N II] and Hα emission lines measurable above the 3σ level (regardless of their [O III] and Hβ emission) and log ([N II]/[Hα]) > -0.2. 13 composite galaxies meet this criterion and we therefore classify these as AGN. The remaining 35 composite galaxies do not meet any of the requirements for AGN selection, and so we classify these as star-forming systems.

Having classified 317 out of 1114 galaxies as star forming or AGN based on the emission-line diagnostic diagram, we attempt to

[2] *http://www.lam.oamp.fr/arnouts/LE_PHARE.html*
[3] M. Polletta (private communication).

classify the remaining 797 galaxies which do not have emission-line detections above 3σ accuracy in 'all four lines' (i.e. [O III], Hα, Hβ and [N II]).

We again use the emission-line criterion for AGN classification of Miller et al. (2004) which requires only [N II] and Hα lines measurable at above 3σ accuracy. We find 162 of these 797 galaxies meet this criterion, and so we classify these as AGN. For the remaining sources to be classified as star-forming systems, they must have Hα measurable at above 2σ accuracy. 214 galaxies meet these criteria. The remaining 421 galaxies could not be classified using emission-line diagnostics. This class consists of galaxies with no or very weak emission lines, and is therefore likely to consist of galaxies with quiescent emission.

Having used emission-line ratios to classify sources in our sample, we find a total of 187 galaxies to have an AGN component, 506 galaxies to be star-forming systems, and 421 galaxies with quiescent emission.

5 OPTICAL COLOUR–MAGNITUDE RELATION

Fig. 2(a) illustrates rest-frame $(g - r)$ colour as a function of r-band absolute magnitude for our spectroscopic sample. Red sequence early-type galaxies and blue sequence late-type galaxies are initially defined by adopting the colour–magnitude relation (CMR) line of Bell et al. (2003). We find two-thirds of our sample contain galaxies with red optical colours and the remaining one-third have blue optical colours (Table 1).

We use SDSS morphological (C_r) and spectral (eClass) classifiers to determine the fraction of early- and late-type galaxies in each sequence (Figs 2b and c). The distribution of our galaxy sample is found to show a continuous trend in classifiers C_r and eClass (Fig. 2c).

Approximately 70 per cent of red sequence galaxies are defined as early type according to both C_r and eClass (red filled circle).

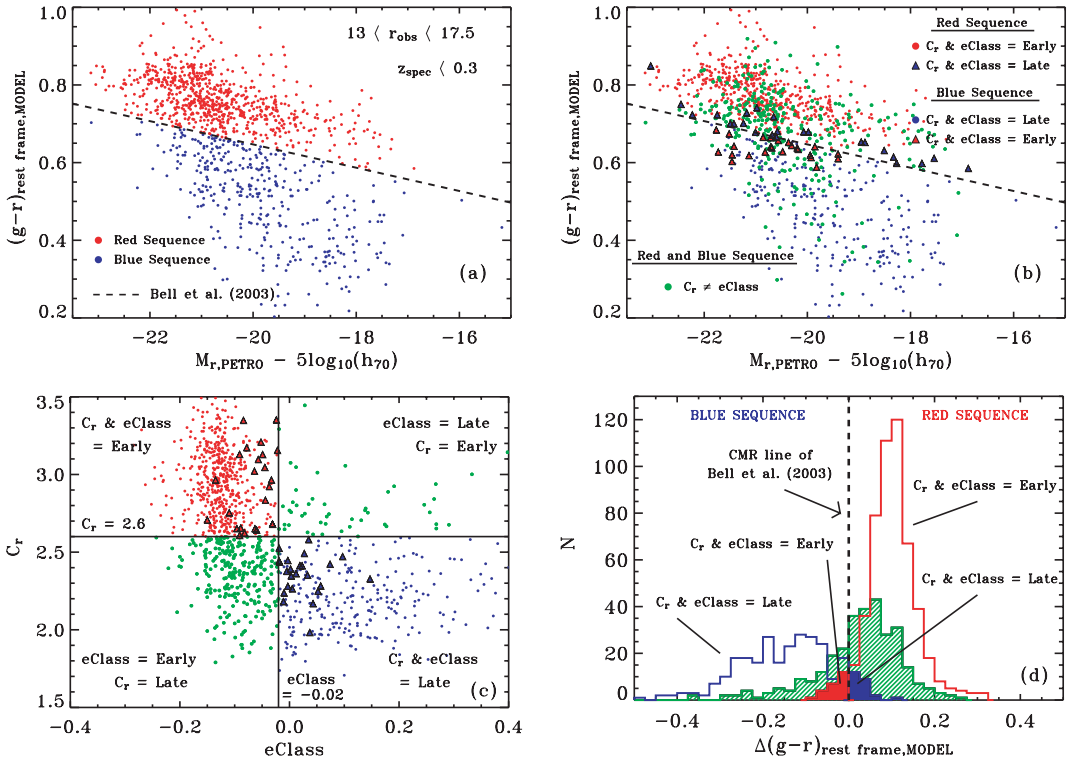

Figure 2. The distribution of SWIRE/SDSS galaxy populations; (a) rest-frame $(g - r)$ colour (magnitudes in AB) of 1114 galaxies against the absolute magnitude in r band, $M_{r,\mathrm{PETRO}}$ - 5 $log_{10}(h_{70})$. The colour criterion for selection of red and blue sequence galaxies is illustrated by the CMR line of Bell et al. (2003) (dashed line). (b) Rest-frame $(g - r)$ colour against the absolute magnitude in r band, showing the classification of galaxies according to C_r and eClass; red sequence early type (red filled circle), red sequence late type (blue filled triangle), blue sequence early type (red filled triangle), blue sequence late type (blue filled circle) and disagreement between C_r and eClass (green filled circle). (c) Distribution of galaxy populations in terms of C_r and eClass. (d) The $(g - r)$ colour of the galaxy populations with respect to the CMR line of Bell et al. (2003).

Table 1. SDSS morphological (concentration index C_r) and spectral classification (eClass) for sources in the red and blue sequence.

Sequence	No.	C_r		eclass		C_r = eClass		$C_r \neq$ eClass
		early	late	early	late	early	late	
Red	741	70 per cent	30 per cent	95 per cent	5 per cent	69 per cent	3 per cent	28 per cent
Blue	373	16 per cent	84 per cent	22 per cent	78 per cent	6 per cent	68 per cent	26 per cent

Similarly, 70 per cent of blue sequence galaxies are defined as late type (blue filled circle). As illustrated by Fig. 2(b), only 3 per cent of galaxies in the red sequence are late type (blue triangle) and 6 per cent of galaxies in the blue sequence are defined as early type (red triangle) according to both classifiers. These galaxies make up less than 4 per cent of the entire spectroscopic sample, and also lie near the boundaries of the classifiers C_r and eClass (Fig. 2c). As shown by Fig. 2(d), galaxies in the blue sequence classified as early type are likely to correspond to the tail of the early-type distribution in the red sequence. Likewise, the late-type galaxies in the red sequence correspond to the tail of the late-type distribution in the blue sequence. In terms of their $(g - r)$ colour, these sources lie in a 'transition region' between the two sequences (Figs 2b and d), either side of the CMR line of Bell et al. (2003).

Therefore, the CMR line is found to correspond well to the boundaries of C_r and eClass, and can be used as a reliable separator of red sequence galaxies dominated by early types and blue sequence galaxies dominated by late types.

In Fig. 2(c), galaxies classified as early type (red) and late type (blue) are found to be separated by a population, where the two classifiers C_r and eClass disagree (green circle). These sources make up ∼27 per cent of the SWIRE/SDSS sample, the majority of which are classified as early type according to eClass and late type according to C_r. These sources are distributed throughout both sequences, with the majority (19 per cent of the SWIRE/SDSS sample) located in the red sequence. As shown in Fig. 2(d), they have slightly bluer $(g - r)$ colour than early-type galaxies in the red sequence and a broader distribution (with $\sigma_{\rm green} \sim 0.1$), with a skewed tail which passes through most of the blue sequence. The percentage of these sources found in each sequence is given in Table 1.

To gain another viewpoint of the galaxy populations in our sample, we look at their spectral classifications (Fig. 3) according to the optical spectral line analysis discussed in Section 4. Star-forming systems are found to dominate the blue sequence, while passive galaxy populations dominate the red sequence. However, a significant number of AGN and star-forming galaxies are also found in the red sequence. This may explain why a significant population of galaxies in the red sequence have been classified as eClass early type and C_r late type, as illustrated by Fig. 2.

By investigating the IR colours of optically selected red and blue sequence galaxies in our sample, we can therefore understand the nature of these active systems in the red sequence, as well as the origin of their red optical colours (i.e. old stellar populations or extinction). Such an IR analysis will also help to determine whether the bimodal distribution seen in the optical is too simplistic in its representation of early- and late-type galaxies in the local universe.

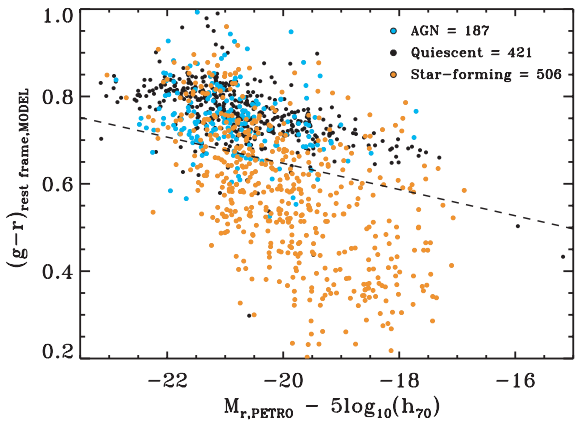

Figure 3. Classification of sources according to the spectral line analysis in Section 4; AGN (cyan), star forming (orange) and galaxies with quiescent emission (black).

6 THE IR COLOUR DISTRIBUTION

Starlight at 3.6 μm can be used to trace the stellar mass distribution of galaxies almost free of dust obscuration effects (i.e. Oliver et al. 2004; Pahre et al. 2004; Franceschini et al. 2006), since any standard extinction law predicts only a small percentage of extinction compared to optical wavelengths.

On the other hand, the study of M51a using *Spitzer* and *HST* (*Hubble Space Telescope*) data has shown directly that 24-μm luminosity can be used as a reliable indicator of obscured star formation (i.e. Calzetti et al. 2005). 24-μm observations of individual H II regions were calibrated against Paα (1.876 μm) observations, which measure the ionized radiation from stars forming in the arms of M51a. A tight linear correlation was found between Paα and 24 μm, proving that the 24-μm dust continuum is a locally accurate tracer of star formation. In addition, the goodness of the mid-IR emission as a star formation tracer at high redshift has been found recently by Marcillac et al. (2006), testing the mid-IR emission against the radio emission of galaxies (see also Elbaz et al. 2002; Gruppioni et al. 2003; Appleton et al. 2004).

We therefore use and interpret IR 3.6-μm luminosity as an indicator of stellar mass and 24 μm luminosity as an indicator of obscured star formation.

In Fig. 4, the ratio $\log(L_{24}/L_{3.6})$ as a function of $\log(L_{24})$ (Fig. 4a) and $\log(L_{3.6})$ (Fig. 4b) are shown for sources in our sample with 24-μm detections (787 sources out of 1114, ∼70 per cent of our sample). L_{24} and $L_{3.6}$ are the luminosities (νL_ν in $L_\odot$) at 24 μm and 3.6 μm. Regions of constant stellar mass are illustrated in Fig. 4(a) by straight dashed lines of constant 3.6-μm luminosity. The stellar mass approximations shown in Fig. 4(a) are based on the SDSS stellar mass catalogue of Kauffmann et al. (2003).

For both red and blue sequence galaxies, the ratio $\log(L_{24}/L_{3.6})$ increases as a function of $\log(L_{24})$. A similar relation between mid-IR (15 μm) and optical luminosities was found to be valid for ISOCAM sources (see La Franca et al. 2004; Pozzi et al. 2004; Rowan-Robinson et al. 2005). In Fig. 4(b), we see that the $\log(L_{24}/L_{3.6})$ ratio of blue sequence galaxies is found to increase with 24-μm luminosity, but $\log(L_{24}/L_{3.6})$ shows little variation with 3.6-μm luminosity. Since $L_{3.6}$ is indicative of stellar mass and L_{24} of star formation rate, the ratio of $\log(L_{24}/L_{3.6})$ can be interpreted as an indication of the level of star formation activity per unit stellar mass or 'specific star formation' (see also Pozzi et al. 2004; Rowan-Robinson et al. 2005). We can then interpret Figs 4(a) and (b) as being determined primarily by two almost independent factors: the stellar mass and the specific star formation.

For red sequence galaxies, the specific star formation is independent of stellar mass. This is clearly seen in Fig. 4(b) where they cluster around $\log(L_{3.6}) \sim 9.8\,L_\odot$ but with a wide range of $\log(L_{24}/L_{3.6})$, and in Fig. 4(a) where the distribution runs parallel to lines of constant stellar mass. The blue sequence galaxies on the other hand appear to have a comparatively constant specific star formation activity, though there is a slight tendency for more massive blue galaxies to have higher specific star formation. This weak trend is in the opposite sense from trends seen in the optical and indicates a more complex relation between the star formation indicators, which we will explore later.

Note that the star formation in red sequence galaxies with very low $\log(L_{24}/L_{3.6})$ ratio is likely to correspond to quiescent rather than

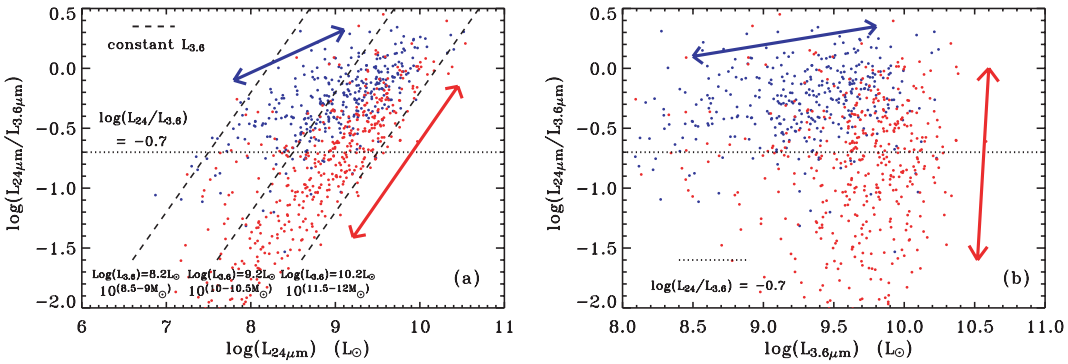

Figure 4. Ratio of 24–3.6 μm luminosity as a function of (a) 24-μm luminosity and (b) 3.6-μm luminosity. Luminosities are in νL_ν. Colours are coded according to Fig. 2(a), where galaxies above the CMR line of Bell et al. (2003) are in red and galaxies below the line are in blue (see Fig. 2a). A cut has been applied at $\log(L_{24}/L_{3.6}) = -0.7$ (dotted line), above which galaxies are dominated by active systems. Dashed lines in Fig. 4(a) signify regions of constant 3.6-μm luminosity. The arrows show the trend of each sequence.

active star formation, due to the interaction between dust and the old stellar populations that exist in these galaxies (Wang & Heckman 1996).

Looking more at luminosities than colours, both red and blue sequence galaxies are found to have similar ranges of 24-μm luminosity ($L_{24} = 10^7$–10^{10} L$_\odot$). Red sequence galaxies are found to have higher 3.6-μm luminosities than galaxies in the blue sequence, which would suggest that galaxies in the red sequence generally have higher stellar mass (10^{10}–10^{12} M$_\odot$) than galaxies in the blue sequence ($10^{8.5}$–10^{11} M$_\odot$).

To separate galaxies with young and evolved star formation, we adopt a cut at $\log(L_{24}/L_{3.6}) = -0.7$, below which the number of blue sequence galaxies is negligible (see Figs 4a and b). Considering sources with 24-μm detections, 92 per cent of galaxies in the blue sequence are above this cut (Table 2), consistent with their nature as actively star-forming systems. However, 44 per cent of red sequence galaxies (195 sources) also have $\log(L_{24}/L_{3.6}) > -0.7$, unexpected of optically red quiescent emitting galaxies.

Table 2. Fraction of red and blue sequence galaxies with $\log(L_{24}/L_{3.6}) > -0.7$ and $\log(L_{24}/L_{3.6}) < -0.7$.

Sequence	No.	24-μm det.	$\log(L_{24}/L_{3.6}) > -0.7$	$\log(L_{24}/L_{3.6}) < -0.7$
Red	741	440	195	245
Blue	373	347	317	30

To make a direct comparison of the optical and IR colours of red and blue sequence galaxies in our sample, we illustrates the ratio $\log(L_{24}/L_{3.6})$ as a function of rest-frame $(g - r)$ colour (Fig. 5a). The $(g - r)$ colour of red sequence galaxies is found to remain constant with increasing $\log(L_{24}/L_{3.6})$ ratio. Red sequence galaxies also have a small spread in $(g - r)$ colour, with $\sigma_{(g-r)} \sim 0.07$. Above our adopted cut of $\log(L_{24}/L_{3.6}) = -0.7$, blue sequence galaxies dominate, and have a larger range of $(g - r)$ colour than red sequence galaxies, with $\sigma_{(g-r)} \sim 0.12$.

To gain a better understanding of the distribution of red and blue sequence galaxies in optical and IR colours, galaxy template tracks are overplotted in Fig. 5(a). The tracks used are from the SWIRE template library. Illustrated is a combination of (i) a 13-Gyr elliptical template and a starburst (M82) template (dot–dashed line), (ii) a 13-Gyr elliptical template and a spiral (Sdm) template (dashed line) and (iii) a 13-Gyr elliptical template and a Seyfert 2 template (dotted line).

Galaxies with low $\log(L_{24}/L_{3.6})$ ratio and red optical colours are dominated by an elliptical template. These galaxies are bulge-dominated systems with quiescent star formation activity.

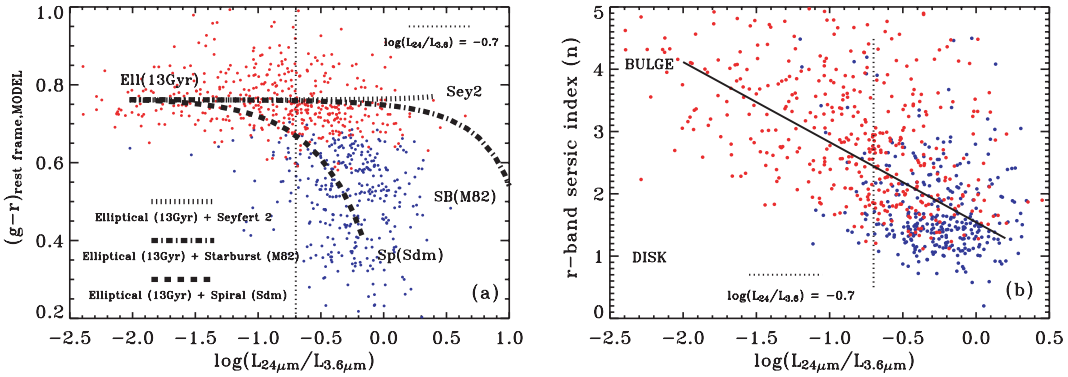

Figure 5. (a) Rest-frame $(g - r)$ colour against the ratio of 24–3.6 μm luminosity. Illustrated are red and blue sequence galaxies with galaxy template tracks overplotted; dot–dashed track = elliptical (13 Gyr) + starburst (M82) template, dashed track = elliptical (13 Gyr) + spiral (Sdm) template, dotted track = elliptical (13Gyr) + Seyfert 2 template. The tracks show that the disc-like contribution from the late-type templates (spiral, starburst and Seyfert 2) increase with $\log(L_{24}/L_{3.6})$ ratio, while the bulge-like contribution from the early-type template (elliptical) decreases. (b) SDSS r-band Sérsic index against the ratio of 24–3.6 μm luminosity. A linear fit to the distribution of the data is illustrated (solid line).

As the ratio $\log(L_{24}/L_{3.6})$ increases, the contribution from the late-type templates increases at varying rates. Galaxies with blue optical colours are completely disc-dominated systems where the optical and IR emission comes from a spiral galaxy. Galaxies with red optical colours and $\log(L_{24}/L_{3.6}) > -0.7$ are found to have up to a 80 per cent AGN or 10 per cent starburst contribution. Galaxies with an AGN owe their red optical colours to their bulge component and their high $\log(L_{24}/L_{3.6})$ ratio to dust heated by the AGN. Extinction could account for the red optical colours of galaxies with a starburst component. However, we find that these systems can have up to a 90 per cent elliptical contribution, where their red optical colours could be due to a significant bulge component (i.e. old rather than reddened stars). Since these systems can have up to a 10 per cent starburst contribution, the high $\log(L_{24}/L_{3.6})$ ratio of these galaxies would correspond to intense bursts of star formation activity. Analysing the optical and IR colours of galaxies in our sample, we therefore observe a possible trend in bulge-to-disc ratio as a function of $\log(L_{24}/L_{3.6})$ colour.

To test whether there is a relationship between the morphology and the IR emission of galaxies in our sample, we analyse their bulge-to-disc ratio (Sérsic index; Sersic 1968) as a function of IR $\log(L_{24}/L_{3.6})$ colour (Fig. 5b). We use the SDSS r-band Sérsic indices (see Section 2.3) as measured by Blanton et al. (2003) for SDSS galaxies.

A correlation is found between Sérsic index and the IR colours of galaxies. Rojas et al. (2004) find that galaxies with $n < 1.8$ have surface brightness profiles that resemble spiral galaxies, while galaxies with $n > 1.8$ are more like ellipticals. We find that red sequence galaxies with low $\log(L_{24}/L_{3.6})$ ratio have a high Sérsic index ($n > 2$) and are bulge-dominated early-type systems. The majority of galaxies with $\log(L_{24}/L_{3.6}) > -0.7$ are found to have a low Sérsic index ($n < 1.5$), and are blue sequence disc-dominated systems. However, red sequence galaxies with $\log(L_{24}/L_{3.6}) > -0.7$ have a Sérsic index >1.5, indicating that they are bulge dominated. For galaxies with an AGN contribution based on the spectral analysis, the bulge component would account for the high Sérsic index. For galaxies with only a starburst component based on the spectral analysis, the red optical colours could be accounted for by a bulge component, and the high mid-IR emission characterized by bursts of star formation from a disc component.

7 RED SEQUENCE GALAXIES WITH HIGH IR EMISSION

Galaxies exhibiting red optical colours and high IR luminosities can be considered either AGN or massive dust-enshrouded starburst galaxies (Bell et al. 2005). Based on the spectral classifications of our sample (see Section 4), 78 of the 195 red sequence galaxies with $\log(L_{24}/L_{3.6}) > -0.7$ contain an AGN component, and 117 galaxies are star-forming systems.

In this section, we further investigate this subsample of galaxies, to determine whether dust obscuration is responsible for the red optical colours of the star-forming galaxies, and whether the integrated optical and IR luminosities of these systems differ from optically red quiescent galaxies and star-forming galaxies with blue optical colours.

7.1 Optical extinction of star-forming galaxies

We have already corrected our optical magnitudes for galactic foreground obscuration when determining rest-frame optical colours (see Fig. 2a). However, obscuration by dust intrinsic to star-forming galaxies can affect the optical colours of a galaxy.

At optical wavelengths, the Balmer decrement (consisting of Balmer line ratios Hα/Hβ) can provide a measure of extinction for optical spectra due to intrinsic reddening (down to an optical depth $\tau \sim 1$), in galaxy regions where bursts of star formation are located (Ward et al. 1987; Calzetti et al. 2005).

To determine the Balmer Decrement, we first apply corrections for stellar absorption to our Hα and Hβ flux measurements. Balmer emission lines sit on top of stellar absorption due to the presence of young and intermediate age stars in the line-emitting galaxy. Therefore, Balmer emission lines uncorrected for this absorption can cause an overestimation in the obscuration measurements derived from the Balmer decrement (Hopkins et al. 2003).

To obtain accurate measures of extinction, we consider galaxies with Hα and Hβ emission greater than 3σ accuracy. For sources with H$\alpha > 3\sigma$ accuracy, but with H$\beta < 3\sigma$, we set the Hβ flux to its 3σ error value. This will allow us to obtain a lower limit measure of the extinction of these sources (see e.g. Babbedge, Whitaker & Morris 2004).

The intrinsic colour excess $E(B-V)_i$ for a uniform screen of dust is related to the Balmer line ratio Hα/Hβ, according to (e.g. Hummer & Storey 1987; Calzetti, Kinney & Storchi-Bergmann 1994)

$$E(B-V)_i \approx 0.935 \ln\left(\frac{\mathrm{H}\alpha/\mathrm{H}\beta}{2.88}\right). \quad (1)$$

We compare the intrinsic colour excess $E(B-V)_i$ of all star-forming galaxies in our sample with $\log(L_{24}/L_{3.6}) > -0.7$; 117 red sequence galaxies and 281 blue sequence galaxies. Fig. 6 shows $E(B-V)_i$ for our two populations of star-forming galaxies, with median values given in Table 3.

After applying an extinction correction to the star-forming galaxies in the red sequence, we find ∼51 per cent of the sample (60 sources) now have optical colours consistent with blue sequence galaxies. These sources are found to have an extinction of $E(B-V)_i \geqslant 0.3$, similar to previous mid-IR selected sources (i.e. Poggianti

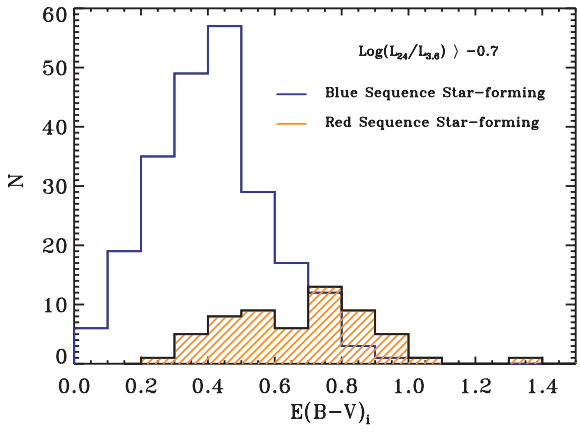

Figure 6. Colour excess $E(B-V)_i$ of red sequence (orange) and blue sequence (blue) star-forming galaxies with $\log(L_{24}/L_{3.6}) > -0.7$.

Table 3. Median colour excess $E(B-V)_i$ of star-forming galaxies with $\log(L_{24}/L_{3.6}) > -0.7$.

Sequence	Median $E(B-V)_i$	St. Dev.
Red	0.70	0.27
Blue	0.41	0.19

& Wu 2000; Pozzi et al. 2003). An $E(B-V)_i < 0.3$ is not found to be sufficient to change the optical colours of these sources. The remaining 49 per cent of the sample (57 sources) either have $E(B-V)_i < 0.3$ or a value of $E(B-V)_i$ could not be determined because Hα did not meet the 3σ emission criteria. This would indicate that these remaining systems are either so extinct that their Balmer lines have been suppressed, or that they are early-type systems characterized by weak Balmer emission.

Since we are measuring extinction values based on emission lines, we are in effect applying an extinction correction based on the star-forming regions of a galaxy rather than the average extinction of the galaxy as a whole. If the red optical colours of star-forming galaxies are due to a bulge component, while intense bursts of star formation activity are due to a disc component, such a disc component may lead to over corrections for extinction, which may disguise the fact that the red optical colour of the galaxy is due to a bulge contribution (i.e. old stellar populations).

7.2 Comparison of optical and IR luminosities

Red sequence star-forming galaxies with $\log(L_{24}/L_{3.6}) > -0.7$ are found to have similar optical colours as early-type galaxies, whereas their IR colours most resemble that of late-type galaxies. We therefore compare the optical and IR SEDs of these systems with those of galaxies in the red and blue sequence as a whole, in terms of rest-frame optical and IR luminosities (see Section 3).

Figs 7(a) and (b) show the optical and IR luminosity distributions of our sample. Red sequence galaxies with quiescent star formation activity (red) are generally found to have higher optical luminosities than blue sequence star-forming galaxies. Star-forming galaxies with red optical colours (orange) and $\log(L_{24}/L_{3.6}) > -0.7$ are not only found to have a similar optical luminosity distribution as bulge-dominated quiescent red sequence galaxies, but optical luminosities that are higher than the majority of star-forming galaxies in the blue sequence.

The IR luminosity distribution of red sequence galaxies is on average found to be lower than that of star-forming galaxies in the blue sequence, since much of the IR activity in the red sequence is due to quiescent star formation. However, approximately a quarter of red sequence galaxies are found to have IR luminosities higher than the majority of star-forming galaxies in the blue sequence. These galaxies either have an AGN contribution, where dust heated by the AGN accounts for their high IR luminosities, or are undergoing intense star formation activity.

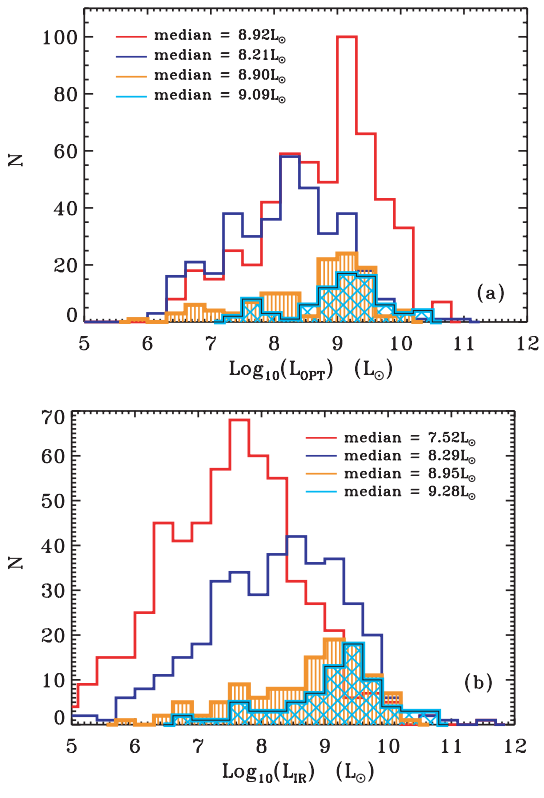

Figure 7. (a) Optical ($L_{\rm OPT}$) and (b) IR ($L_{\rm IR}$) luminosity distributions of quiescent red sequence galaxies (red) and active blue sequence galaxies (blue). Also shown is the luminosity distribution of red sequence galaxies with $\log(L_{24}/L_{3.6}) > -0.7$ classified as either star forming (orange) or AGN (cyan) based on the spectral line analysis.

7.3 SWIRE_J104152.92 + 595616.3

Fig. 8 shows an example of a red sequence star-forming galaxy at $z \sim 0.147$ with $\log(L_{24}/L_{3.6}) > -0.7$. This galaxy has a Sérsic index $\sim$3.6 (see Section 6) and the SDSS and 3.6-μm SWIRE images (Fig. 8a) show a bulge component which would account for its red optical colour. However, this galaxy is also found to have strong mid- to far-IR emission as illustrated at 70 μm ($f_{70\,\mu\rm m} \sim 30$ mJy). We model the optical and IR SED of this galaxy using the SWIRE template library (Fig. 8b). We have already shown using spectral line diagnostics (see Section 4) that these galaxies are not contaminated by AGN. Therefore, as a test, we attempt to model the IR SED of this galaxy as Seyfert 2 AGN (green), and find that doing so would significantly overestimate its far-IR emission. We find the IR SED is best modelled as a spiral – Sc (blue), which would agree with the fact that these systems have high IR emission as a result of bursts of star formation activity.

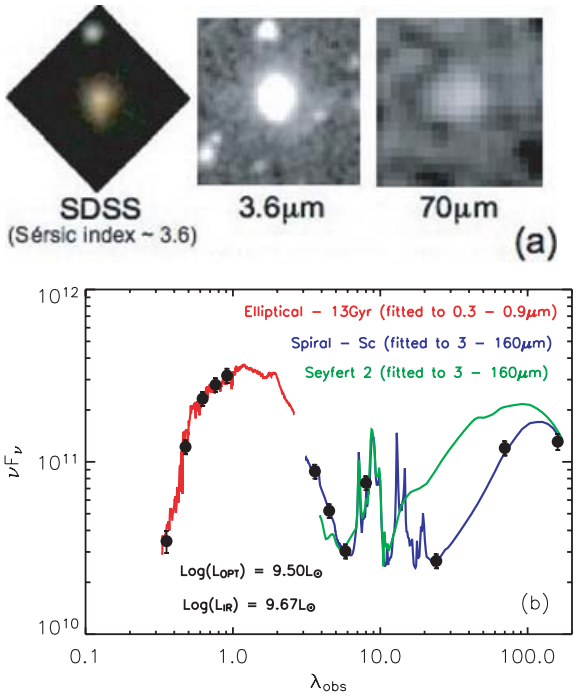

Figure 8. SWIRE_J104152.92+595616.3: example of red sequence star-forming galaxy with $\log(L_{24}/L_{3.6}) > -0.7$. (a) SDSS optical image, 3.6- and 70-μm SWIRE images. (b) The optical and IR SED modelled with SWIRE galaxy templates.

The optical SED of this galaxy is found to resemble that of a 13-Gyr elliptical template (red), and the IR SED best modelled by a Spiral template (blue). This galaxy did not meet the 3σ emission-line criteria (see Section 7.1) required for determining an estimate of extinction using the Balmer decrement. As mentioned in Section 7.1, this could be due to the fact that either the galaxy is so extinct that its Balmer lines have been suppressed, or the galaxy is characterized by weak Balmer emission. The high optical luminosity of this system, a surface brightness profile resembling an elliptical galaxy (i.e. a Sérsic index >1.8) and an optical SED best modelled as an elliptical are indications that the red optical colours of such systems are mainly a result of a bulge component rather than substantial reddening.

8 THE NUMBER DENSITY AND LUMINOSITY DENSITY OF RED AND BLUE SEQUENCE GALAXIES

Star-forming galaxies are expected to provide a major contribution to both the number density and optical/IR luminosity densities of blue sequence galaxies. In comparison, the majority of red sequence galaxies undergoing quiescent star formation activity will account for the number density and optical luminosity density of the red sequence, providing less of a contribution to the IR luminosity density than more active systems. However, IR colours have shown that a quarter of red sequence galaxies in our sample are active systems, and must therefore provide a significant contribution to both the number density and luminosity density of the local universe.

We therefore determine the integrated number density – total of $1/V_{\rm max}$ (Schmidt et al. 1968; Felten 1976) of galaxies in the red and blue sequence and compare with the number density of AGN and star-forming galaxies with red optical colours and $\log(L_{24}/L_{3.6}) > -0.7$. $V_{\rm max_i}$ is the volume corresponding to the maximum redshift at which a source could be detected by the survey. We set this maximum redshift by considering optical and IR limits, determined using *k*-corrections calculated for each galaxy from its optical and IR template fits (see Section 3).

For each galaxy, the density contribution $1/V_{\rm max_i}$ and the luminosity contribution $L_i/V_{\rm max_i}$ are computed. We correct for incompleteness as a result of the spectroscopic cuts in ZWARNING and zConf (see Section 2.2).

Table 4 shows the number and luminosity densities of red and blue sequence galaxies in our sample. Galaxies with red optical colours and $\log(L_{24}/L_{3.6}) < -0.7$ account for more than two-thirds of the number density and optical luminosity density of red sequence galaxies. These sources make up more than half the number density and more than two-thirds of the optical luminosity density of our total galaxy sample. In contrast, these galaxies account for only 17 per cent of the total IR luminosity density due to their quiescent star formation activity.

Whereas the number density and optical luminosity density of our galaxy sample is dominated by red sequence galaxies with quiescent star formation, the contribution to the IR luminosity density comes from a number of populations in both the red and blue sequences. Star-forming galaxies account for more than 90 per cent of the IR luminosity density of the blue sequence, and 34 per cent of the IR luminosity density of our total galaxy sample. These systems account for only 2 per cent of the total optical luminosity density.

We find that active systems (AGN and star-forming galaxies) in the red sequence account for a quarter of the total number density of our galaxy sample: AGN representing 11 per cent and star-forming galaxies 13 per cent.

Thermal dust emission from red sequence AGN contributes $\sim$19 per cent to the total IR luminosity density. Due to intense bursts of star formation activity, red sequence star-forming galaxies contribute $\sim$28 per cent to the IR luminosity density of our SWIRE/SDSS sample. In addition, the optical luminosity density of these star-forming systems is found to be eight times greater than that of star-forming galaxies in the blue sequence.

9 DISCUSSION AND CONCLUSIONS

We present the analysis of the rest-frame optical and IR colours of 1114 $z < 0.3$ galaxies from the SWIRE survey and the SDSS.

We separate our sample into two populations. Based on rest-frame $(g - r)$ colour, galaxies with red optical colours are defined as 'red sequence galaxies'. Galaxies with blue optical colours are defined as 'blue sequence galaxies'.

To test whether the bimodal sequence seen using rest-frame optical colours represent a simple division of early and late-type galaxies in the local universe, we analyse their optical spectra to identify quiescent and active (starburst and AGN) systems and use IR $\log(L_{24}/L_{3.6})$ colour to investigate the star formation activity of each sequence as a function of stellar mass.

We find red sequence galaxies have a broad range of star formation activity independent of their stellar mass. Galaxies with weak star formation appear to be bulge-dominated early-type systems, whereas those with higher levels of activity have a contribution

Table 4. Number density and luminosity density of red and blue sequence galaxies. Number and luminosity densities as a percentage of the sample total are given in brackets.

Sequence	$\log(L_{24}/L_{3.6}) < -0.7$	$\log(L_{24}/L_{3.6}) > -0.7$ (AGN)	$\log(L_{24}/L_{3.6}) > -0.7$ (star forming)	Sequence total (h^3 Mpc^{-3})	Sample total (h^3 Mpc^{-3})
			Number density		
Red	69 per cent (55 per cent)	14 per cent (11 per cent)	17 per cent (13 per cent)	3.5×10^{-6}	(4.4×10^{-6})
Blue	10 per cent (2 per cent)	7 per cent (1 per cent)	83 per cent (18 per cent)	8.9×10^{-7}	
			Optical luminosity density		
Red	69 per cent (67 per cent)	15 per cent (15 per cent)	16 per cent (16 per cent)	5.6×10^3 L$_\odot$	$(6.8 \times 10^3$ L$_\odot)$
Blue	13 per cent (<1 per cent)	6 per cent (<1 per cent)	81 per cent (2 per cent)	1.2×10^3 L$_\odot$	
			IR luminosity density		
Red	27 per cent (17 per cent)	29 per cent (19 per cent)	44 per cent (28 per cent)	3.8×10^3 L$_\odot$	$(6.1 \times 10^3$ L$_\odot)$
Blue	1 per cent (<1 per cent)	6 per cent (2 per cent)	93 per cent (34 per cent)	2.3×10^3 L$_\odot$	

from both a bulge and disc component. In comparison, galaxies in the blue sequence are found to have high levels of activity, resembling disc-dominated spiral-like systems.

We therefore postulate that the $(g - r)$ colour and $\log(L_{24}/L_{3.6})$ colour of galaxies in our sample are determined primarily by a bulge-to-disc ratio. This relationship is perhaps more continuous than is perceived when viewed in the projection of one colour, and is such that the $(g - r)$ colour is sensitive to the bulge-to-disc ratio for disc-dominated galaxies, whereas the $\log(L_{24}/L_{3.6})$ colour is sensitive to bulge-to-disc ratio for bulge-dominated systems.

We find a significant fraction of our red sequence sample ($\sim$26 per cent, 195 sources) with intrinsic red optical colours and high $\log(L_{24}/L_{3.6})$ ratio. These systems are characterized as either AGN (78 sources) or systems with bursts of star formation activity (117 sources). AGN owe their red optical colours to their bulge component, and their high $\log(L_{24}/L_{3.6})$ ratio would be due to dust heated by AGN. Using galaxy template models, star-forming galaxies in the red sequence are found to have up to a 90 per cent elliptical contribution and a 10 per cent starburst contribution. The red optical colours of these systems would therefore be due to a bulge component, and their high $\log(L_{24}/L_{3.6})$ ratio would correspond to intense star formation activity accounted for by a disc component.

Extinction could in principle account for the red optical colours of approximately half of these star-forming galaxies. However, such corrections for extinction are based on the star-forming regions of a galaxy rather than the average extinction of the galaxy as a whole. If these systems are undergoing localized bursts of star formation activity, this would lead to overcorrections for extinction, which may disguise the fact that the red optical colours of these star-forming galaxies are actually due to a significant bulge component.

To gain a better understanding of the nature of these red sequence star-forming galaxies, we compare their optical and IR luminosities with that of red and blue sequence galaxies as a whole. These systems are found to have optical luminosities resembling that of bulge-dominated red sequence galaxies with quiescent star formation, whereas intense bursts of star formation activity means their IR luminosities are on average higher than the majority of star-forming galaxies in the blue sequence. This confirms our suspicion that these galaxies have significant bulge components and are not pure disc-like galaxies with high levels of extinction.

It has been postulated that the recent evolution of early-type galaxy populations can be explained by a 'dry mergers scenario' (see e.g. Toomre & Toomre 1972; Bell et al. 2006), where non-star-forming galaxies merge to form massive early-type systems. Early studies of galaxy morphology and density in rich clusters (Dressler 1980; Postman & Geller 1984) have also shown that the large bulge-to-disc ratio commonly associated with early-type galaxies is inconsistent with the idea that such systems are the progenitors of disc-dominated late-type galaxies. More recent studies have shown that star-forming spiral–spiral mergers could result in the formation of early-type galaxies at low optical luminosities (Naab, Khochfar & Burkert 2006). However, semi-analytic work by Khochfar & Burkert (2003, 2005) and optical survey studies by van Dokkum et al. (1999), Tran et al. (2005) and Bell et al. (2005) have suggested that there are relatively few optically blue star-forming galaxies in the low-redshift universe luminous enough to merge into present day massive early-type galaxies, favouring the dry mergers scenario. Our results suggest that there is a substantial population of massive, red, galaxies with ongoing star formation activity. This may reduce the need for dry mergers.

We finally quantify the contribution of these dusty star-forming galaxies to optically selected galaxies in the local universe. Red sequence galaxies make up 79 per cent of the total number density of our sample. 83 per cent of blue sequence galaxies and 17 per cent of red sequence galaxies are found to be actively star-forming systems. Most of the optical luminosity density (67 per cent) is due to quiescent red sequence galaxies and less than 4 per cent to galaxies in the blue sequence. Star-forming galaxies are found to have a similar contribution to the optical luminosity density of the red sequence as AGN. Red sequence AGN and quiescent galaxies are responsible for 36 per cent of the total IR luminosity density. Active star-forming galaxies produce 62 per cent of the total IR luminosity density of our SWIRE/SDSS sample, of which 28 per cent is as a result of star-forming galaxies in the red sequence.

ACKNOWLEDGMENTS

PD is supported by a PPARC studentship (PPA/S/S/2002/03500/), SJO is supported by a Leverhulme Research Fellowship, SJO and IW are supported by PPARC standard grant (PPA/G/S/2000/00508 and PPA/G/S/2002/00481). We thank Jon Loveday for his advice on certain aspects of the SDSS data. We thank the referee Randall Rojas for his helpful comments and suggestions. The support for this work, part of the Spitzer Space Telescope Legacy Science Program, was provided by NASA through an award issued by the Jet Propulsion Laboratory, California Institute of Technology under the NASA contract 1407.

REFERENCES

Abazajian K. et al., 2004, AJ, 128, 502
Appleton P. N. et al., 2004, ApJS, 154, 147
Babbedge T. S. R., Whitaker R., Morris S., 2004, MNRAS, 353, 654
Baldry I. V., Glazebrook K., Brinkmann J., Ivezic Z., Lupton R. H., Nichol R. C., Szalay A. S., 2004, ApJ, 600, 681
Baldwin A., Phillips M. M., Terlevich R., 1981, PASP, 93, 817
Bell E. F., McIntosh D. H., Katz N., Weinberg M. D., 2003, ApJ, 149, 289
Bell E. F. et al., 2004, ApJ, 608, 752
Bell E. F. et al., 2005, ApJ, 625, 23
Bell E. F. et al., 2006, ApJ, 640, 241
Bertin E., Arnouts S., 1996, A&AS, 117, 393
Blanton M. R. et al., 2001, ApJ, 121, 2358
Blanton M. R. et al., 2003, ApJ, 594, 186
Blanton M. R. et al., 2004, AJ, 129, 2562
Brinchmann J., Charlot S., White S. D. M., Tremonti C., Kauffmann G., Heckman T., Brinkmann J., 2004, MNRAS, 351, 1151
Bruzual A., Charlot S., 1993, ApJ, 405, 538
Calzetti D., Kinney A. L., Storchi-Bergmann T., 1994, ApJ, 429, 582
Calzetti D. et al., 2005, ApJ, 633, 871
Cimatti A. et al., 2004, Nat, 430, 184
Connolly A. J., Szalay A. S., 1999, AJ, 117, 2052
Connolly A. J., Szalay A. S., Bershady M. A., Kinney A. L., Calzetti D., 1995, AJ, 110, 1071
Dale D. A., Helou G., 2002, ApJ, 576, 159
Dressler A., 1980, ApJ, 236, 351
Elbaz D. et al., 1999, A&A, 351, 37
Elbaz D., Flores H., Chanial P., Mirabel I. F., Sanders D., Duc P. A., Cesarsky C. J., Aussel H., 2002, A&A, 381, 1
Fazio G. et al., 2004, ApJS, 154, 10
Felten J. E., 1976, ApJ, 207, 700
Flores H., Hammer F., Elbaz D., Cesarsky C. J., Liang Y. C., Fadda D., Gruel N., 2004, A&A, 415, 885
Franceschini A. et al., 2006, A&A, 453, 397
Frayer D. T. et al., 2006, AJ, 131, 250
Giallongo E., Salimbeni S., Manci N., Zamorani G., Fontana A., Dickinson M., Cristiani S., Pozzetti L., 2005, ApJ, 622, 116

Gruppioni C., Lari C., Pozzi F., Zamorani G., Franceschini A., Oliver S., Rowan-Robinson M., Serjeant S., 2002, MNRAS, 335, 831
Gruppioni C., Pozzi F., Zamorani G., Ciliegi P., Lari C., Calabrese E., La Franca F., Matute I., 2003, MNRAS, 341, 1
Hatton S., Devriendt J. E. G., Ninin S., Bouchet F. R., Guiderdoni B., Vibert D., 2003, MNRAS, 343, 75
Hogg D. W. et al., 2004, ApJ, 601, 29
Hopkins A. M. et al., 2003, ApJ, 599, 971
Hummer D. G., Storey P. J., 1987, MNRAS, 224, 801
Ilbert O. et al., 2005, A&A, 439, 863
Kauffmann G. et al., 2003, MNRAS, 341, 33
Kessler M. F. et al., 1996, A&A, 315, 27
Kewley L. J., Dopita M. A., Sutherland R. S., Heisler C. A., Trevena J., 2001, ApJ, 556, 121
Khochfar S., Burkert A., 2003, ApJ, 597, 117
Khochfar S., Burkert A., 2005, MNRAS, 359, 1379
Kron R. G., 1980, ApJS, 43, 305
La Franca F. et al., 2004, AJ, 127, 3075
Lonsdale C. et al., 2003, PASP, 115, 897
Lonsdale C., Farrah D., Smith H. E., 2006, A&A, in press (astro-ph/0603031)
Marcillac D., Elbaz D., Chary R. R., Dickinson M., Galliano F., Morrison G., 2006, A&A, 451, 57
McIntosh D. H. et al., 2005, ApJ, 632, 191
Metcalfe L., Fadda D., Biviano A., 2005, Space Sci. Rev., 119, 425
Miller C. J., Nichol R. C., Gomez P. L., Hopkins A. M., Bernardi M., 2004, ApJ, 597, 142
Naab T., Khochfar S., Burkert A., 2006, ApJ, 636, 81
Neugebauer G. et al., 1984, ApJ, 278, L1
Oliver S. et al., 2004, ApJS, 154, 30
Pahre M. A., Ashby M. L. N., Fazio G. G., Willner S. P., 2004, ApJS, 154, 235
Poggianti B. M., Wu H., 2000, ApJ, 529, 157
Postman M., Geller M. J., 1984, ApJ, 281, 95
Pozzi F. et al., 2003, MNRAS, 343, 1348
Pozzi F. et al., 2004, ApJ, 609, 122
Rieke G. H. et al., 2004, ApJS, 154, 25
Rigopoulou D. et al., 2000, ApJ, 537, L85
Rojas R. R., Vogeley M. S., Hoyle F., Brinkmann J., 2004, ApJ, 617, 50
Rowan-Robinson M. et al., 2004, MNRAS, 351, 1290
Rowan-Robinson M. et al., 2005, AJ, 129, 1183
Sanders D. B., Ishida C. M., Mazzarella J. M., Veilleux S., Surace J. A., Guyon O., Jensen J. B., Kim D. C., 2004, in Storchi Bergman Th., Ho L. C., Schmitt H. R., eds, IAU Symp. 222, The Interplay among Black Holes, Stars and ISM in Galactic Nuclei. Cambridge Univ. Press, Cambridge, p. 477
Saunders D. B., Mirabel I. F., 1996, ARA&A, 34, 749
Schlegel D. J., Finkbeiner D. P., Douglas P., Davis M., 1998, ApJ, 500, 525
Schmidt M., 1968, ApJ, 151, 393
Seaton M. J., 1979, MNRAS, 187, 73
Sersic J. L., 1968, Atlas de Galaxias Australes. Cordoba Obs. Astron., Cordoba
Shimasaku K. et al., 2001, AJ, 122, 1238
Soifer B. T., Neugebauer G., 1991, AJ, 101, 354
Stoughton C. et al., 2002, AJ, 123, 485
Strateva I. et al., 2001, AJ, 122, 1861
Strauss M. A. et al., 2002, AJ, 124, 1810
Surace J. et al., 2005, SWIRE Data Release 2 Document
Toomre A., Toomre J., 1972, ApJ, 178, 623
Tran K. V. H., van Dokkum P., Franx M., Illingworth G. D., Kelson D. D., Forster Schreiber N. M., 2005, ApJ, 627, 25
van Dokkum P. G., Franx M., Fabricant D., Kelson D. D., Illingworth G. D., 1999, ApJ, 520, 95
Veilleux S., Osterbrock D. E., 1987, ApJ, 63, 295
Wang B., Heckman T. M., 1996, ApJ, 457, 645
Wang B., Silk J., 1994, ApJ, 427, 759
Ward M. J., Geballe T., Smith M., Wade R., Williams P., 1987, ApJ, 316, 138
Yip C. W. et al., 2004, AJ, 128, 2603
York D. G. et al. (SDSS Collaboration), 2000, AJ, 120, 1579

This paper has been typeset from a TEX/LATEX file prepared by the author.